Med Ultrason 2026, Vol. 28, no. 3, 366-367

Ultrasound was born dynamic: why are we still scanning static?

Ahmad J. Abdulsalam[1], Abdulrazzaq Aldhafiri[2]

[1]Department of Physical Medicine and Rehabilitation, Mubarak Al-Kabeer Hospital, Jabriya, [2]Department of Physical Medicine and Rehabilitation, Physical Medicine and Rehabilitation Hospital, Andalous, Kuwait

To the Editor,

Musculoskeletal ultrasound has one clear advantage over every other imaging modality: real-time, dynamic visualization of moving structures. And yet, the vast majority of published musculoskeletal ultrasound studies, clinical protocols, and training curricula still prioritize static image acquisition. We are using a dynamic tool to produce static answers, and missing diagnoses in the process.

The clinical consequences are real. Snapping syndromes of the hip, subluxation of the biceps tendon or peroneal tendons, dynamic impingement at the shoulder, ulnar nerve instability at the cubital tunnel, and trigger finger can all appear entirely normal on a static ultrasound image [1]. These pathologies only become apparent when the patient moves, yet many sonographic examinations are still performed with the patient lying motionless. A recent review of dynamic musculoskeletal ultrasound in orthopedics highlighted how real-time imaging during movement provides diagnostic information that MRI and CT simply cannot offer, because those modalities are inherently static [2]. This is not a minor point; it is what makes musculoskeletal ultrasound unique, and we are underutilizing it.

Why does static imaging continue to dominate? There are several reasons. First, dynamic assessment takes more time and demands greater operator skill. The clinician must manage the transducer, instruct the patient through provocative maneuvers, and interpret rapidly changing images simultaneously. Second, there is no widely adopted standardized protocol for dynamic maneuvers by body region. Without consensus on what movements to perform, when, and how to document them, practitioners default to what is reproducible: the static image. Third, the research literature reinforces this tendency. Most diagnostic accuracy studies compare ultrasound to MRI using static measurements (thickness, cross-sectional area, echogenicity), overlooking the very dynamic capabilities that set ultrasound apart.

The concept of an "ultrasound examination" that integrates clinical examination with real-time sonographic assessment, described by Pirri et al. as using the transducer as a "magnifying glass" during clinical evaluation, is where musculoskeletal sonography needs to go [3]. Sono-palpation, dynamic stress testing under ultrasound visualization, and real-time guided provocative maneuvers are not advanced techniques reserved for specialists; they should be standard components of every musculoskeletal ultrasound examination. The growing availability of handheld and point-of-care ultrasound devices makes this more practical than it has ever been [4].

We urge the musculoskeletal ultrasound community, and this journal in particular, to take on two initiatives. First, the development of standardized, region-specific dynamic assessment protocols that can be incorporated into existing examination workflows. Second, a change in how we design and report ultrasound studies: diagnostic accuracy papers that omit dynamic assessment should explicitly acknowledge this as a limitation, rather than considering it as an acceptable practice. If we keep measuring ultrasound against MRI using only the parameters at which MRI excels, we will always underestimate the tool in our hands. The musculoskeletal system moves. Our imaging should too.

Received 29.03.2026 Accepted 18.05.2026
Med Ultrason
2026, Vol. 28, No 3, 366-367, DOI: 10.11152/mu-4636,
Corresponding author: Ahmad J. Abdulsalam, MD
Department of Physical Medicine
and Rehabilitation,
Mubarak Al-Kabeer Hospital,
Jabriya, Kuwait
E-mail: dr.ahmad.j.abdulsalam@gmail.com

References

1. Flores DV, Bohyn C, Murray TE, Murphy DT, Cresswell M. Dynamic US of musculoskeletal disorders: a pictorial review with emphasis on techniques. Radiographics 2023;43:e220130.

2. Pan G. Current status of dynamic musculoskeletal ultrasound for application to treatment of orthopedic diseases. Am J Transl Res 2024;16:2180-2189.
3. Pirri C, Pirri N, Stecco C, et al. 'Ultrasound examination' of the musculoskeletal system: bibliometric/visualized analyses on the terminology (change). Tomography 2023;9: 352-361.
4. Sabido-Sauri R, Eder L, Emery P, Aydin SZ. Integrating handheld ultrasound in rheumatology: a review of benefits and drawbacks. Best Pract Res Clin Rheumatol 2025:102085.

A strange mass on the face of the fetus: cutaneous hamartoma

Bi Lei[1,2], Lang Liu[1], Hui Liu[1]

[1]Department of Ultrasound, The Affiliated Hospital of Southwest Medical University, [2]Department of Ultrasound, Gulin County People's Hospital, Luzhou, Sichuan, China

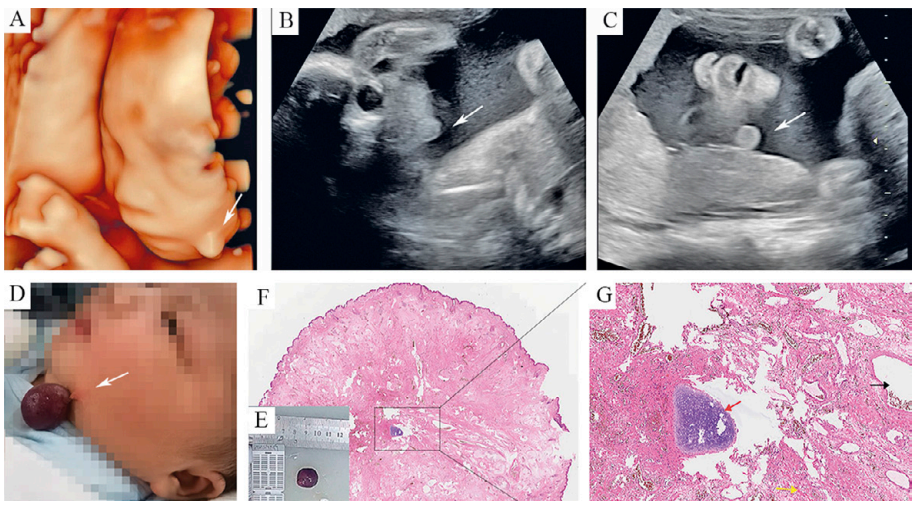


Fig 1. A) Prenatal 3D ultrasound at 23 weeks of gestation showing a left facial mass; B-C) Prenatal 2D ultrasound at 28 weeks of gestation demonstrating a persistent left facial mass; D) Postnatal photograph of the infant; E) Resected left facial mass specimen; F-G) Histopathological examination (H&E staining) revealed multiple tissue components: desmoplasia (G, yellow arrows), hyperplastic/dilated vessels (G, black arrows), and a cartilage nodule (G, red arrows). Abbreviations: 2D, two-dimensional; 3D, three-dimensional.

To the Editor,

A 29-year-old multiparous woman underwent three-dimensional (3D) ultrasound at 22 weeks' gestation, revealing a 15×13 mm isolated, well-circumscribed facial mass (fig 1A). At 28 weeks, two-dimensional (2D) ultrasound showed a homogeneous, solid, isoechoic dermal mass with superficial protrusion (fig 1B-C), with 3D imaging demonstrating slight enlargement to 18×17 mm. Dynamic ultrasound monitoring during pregnancy revealed slow growth of the mass. Following multidisciplinary consultation, vaginal delivery was recommended. The infant was delivered vaginally at 39 weeks of gestation, with Apgar scores 10-10-10. A pedunculated, dark purple mass measuring 20×20 mm was observed immediately after delivery on the left cheek (fig 1D). Postpartum 2D ultrasound revealed that the mass was smooth, homogeneous, and devoid of blood flow signals. Histopathology of the CO_2 laser–excised specimen confirmed congenital facial cutaneous hamartoma (fig 1E-G).

Received 02.06.2026 Accepted 26.07.2026
Med Ultrason
2026, Vol. 28, No 3, 367-368, DOI: 10.11152/mu-4637,
Corresponding author: Hui Liu
Department of Ultrasound,
The Affiliated Hospital of
Southwest Medical University,
Luzhou, Sichuan 646000, China
E-mail: lh009680@swmu.edu.cn

Hamartomas represent localized proliferations of histologically mature native tissue exhibiting architectural disorganization, abnormal cellular proportions, or maturation defects. These lesions typically follow a benign clinical course with limited autonomous growth, most commonly arising in visceral organs (e.g., lungs, kidneys, intestines). Facial occurrence during fetal development is exceptionally rare [1].

2D ultrasound is the preferred and foundational tool for prenatal diagnosis of isolated facial hamartomas in fetuses, offering advantages such as high-resolution structural imaging, multi-planar scanning capability, blood flow assessment, and cost-effectiveness. It provides critical evidence for differential diagnosis. For example, solitary cutaneous hamartomas typically present as localized soft tissue masses without associated abnormalities of intracranial structures [2]. However, for complex cases, it is recommended to combine 2D ultrasound with 3D ultrasound or MRI to further evaluate the tumor's 3D morphology and spatial relationship with surrounding structures, thereby optimizing prenatal counseling and perinatal management strategies [3].

References

1. Coombs PR, Gilbertson T, Teoh M. Prenatal sonographic diagnosis of a congenital oral fibrovascular hamartoma. Ultrasound Obstet Gynecol 2011;37:736-738.
2. Smet M, Shurmer T, Kesby G, McLennan A. Prenatal Diagnosis of a Facial Teratoma. A Proposed Approach to Diagnose Prenatal Facial Anomalies. J Ultrasound Med 2021;40:1743-1748.
3. Sivera R, Clark AE, Dall'Asta A, Ghi T, Schievano S, Lees CC. Fetal face shape analysis from prenatal 3D ultrasound images. Sci Rep 2024;14: 4411.

Endoscopic ultrasound-guided fine-needle aspiration assisted by a novel dental floss traction technique for diagnosing an occult pharyngeal malignancy: a first case report

Yan Dang[1,2*], Sha Zhang[2,*], Yu Bao[2], Chongqing Shi[1], Zhenming Zhang[2]

** the authors share the first authorship*

[1]Department of Nursing, School of Medicine, Wuhan University of Science and Technology, Wuhan, Hubei Province, [2]Department of Endoscopy Center, Sichuan Clinical Research Center for Cancer, Sichuan Cancer Hospital & Institute, Sichuan Cancer Center, Affiliated Cancer Hospital of University of Electronic Science and Technology of China, Chengdu, Sichuan Province, China

To the Editor,

A 66-year-old male presented with a five-month history of a mass in the right side of the neck. The patient subsequently underwent a right cervical lymphadenectomy. Histopathological examination confirmed metastatic squamous cell carcinoma, and immunohistochemistry revealed diffuse P16 positivity. Whole-body positron emission tomography/computed tomography imaging revealed a hypermetabolic nodule (approximately 1.5×1.0 cm) on the right lateral oropharyngeal wall, with no other significant lesions (fig 1a). Endoscopy showed no neoplastic lesions, and the mucosa was completely smooth (fig 1b).

Under general anesthesia, endoscopic ultrasound (EUS) was conducted via a transnasal approach. A hypoechoic nodule (15.7×12.9 mm) with irregular internal echogenicity and relatively regular borders was observed in the right lateral oropharyngeal wall. Due to limited visibility after the insertion of a 22-gauge puncture needle, dental floss traction was used to increase the angu-

Received 17.05.2026 Accepted 26.07.2026
Med Ultrason
2026, Vol. 28, No 3, 368-369, DOI: 10.11152/mu-4638,
Corresponding author: Zhenming Zhang
Department of Endoscopy Center, Sichuan Clinical Research Center for Cancer, Sichuan Cancer Hospital & Institute, Sichuan Cancer Center, Affiliated Cancer Hospital of University of Electronic Science and Technology of China
55, Section 4, Renmin South Road,
Wuhou District, Chengdu 610041,
Sichuan Province, China
E-mail: zhangzhenming85@126.com

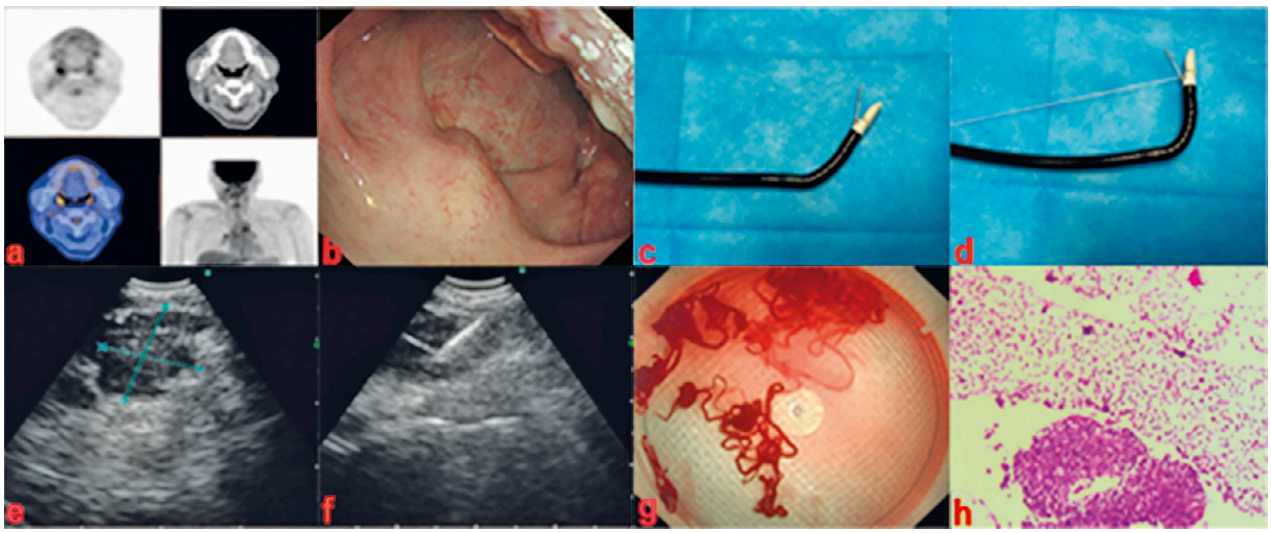


Fig 1. a) PET/CT revealed a hypermetabolic nodule on the right lateral oropharyngeal wall; b) No abnormalities were detected using white light endoscopy; c) The distal end of the echoendoscope with an ultrasonic transducer covered by a water-inflatable balloon, and a 22-gauge needle introduced via the biopsy channel; d) After using the dental floss traction technique, the angle of the endoscopic bending section significantly increased, improving the success rate of puncture at larger angles; e) EUS revealed an irregular mass in the right lateral oropharyngeal wall, measuring 15.7×12.9 mm; f) EUS-FNA was successfully performed with a 22-gauge needle; g) Tissue specimens aspirated during EUS-FNA; h) Pathologically confirmed oropharyngeal squamous cell carcinoma (magnification×200).

lation of the endoscope, thereby enhancing lesion exposure (fig 1c-d). Under EUS guidance, the lesion was punctured (fig 1e-f), and over 20 passes were made to collect adequate tissue samples for histopathology and liquid-based cytology (fig 1g). The procedure was completed without any immediate or delayed bleeding. The final pathological diagnosis confirmed oropharyngeal squamous cell carcinoma (fig 1h), and the patient was referred for chemoradiotherapy.

Oropharyngeal carcinoma is one of the most common head and neck malignancies; however, the submucosal type is rare in clinical practice. Conventional endoscopic biopsy is often insufficient for diagnosing submucosal lesions due to its limited depth of penetration. Endoscopic ultrasound-guided fine-needle aspiration (EUS-FNA) is a safe, effective, and minimally invasive technique commonly used for diagnosing mediastinal and biliary-pancreatic disorders [1]. In this case, EUS-FNA was successfully employed to sample a small submucosal oropharyngeal malignancy. Moreover, dental floss traction, commonly used in endoscopic resection of gastrointestinal tumors, was adapted to improve visualization in a technically challenging anatomical site [2-3]. This maneuver improved lesion exposure, allowing for accurate sampling and a definitive diagnosis.

References

1. Dumonceau JM, Deprez PH, Jenssen C, et al. Indications, results, and clinical impact of endoscopic ultrasound (EUS)-guided sampling in gastroenterology: European Society of Gastrointestinal Endoscopy (ESGE) Clinical Guideline - Updated January 2017. Endoscopy 2017;49:695-714.
2. Tamari H, Oka S, Kotachi T, et al. Indications for dental floss clip traction during gastric endoscopic submucosal dissection by less-experienced endoscopists. J Gastric Cancer 2023;23:512-522.
3. Luo H, Tang J, He X, Shi Y, Chang Y. Efficacy and prognosis analysis of pulley traction-assisted endoscopic submucosal dissection with dental floss for early gastric cancer and precancerous lesions. Front Surg 2025;12:1477658.

A neck mass suspected to be a branchial cleft cyst: a case of macrocystic lymphatic malformation

Peihai Sun[1], Yihua Gao[1], Kuichang Yuan[2]

[1]Department of Medical Ultrasound, [2]Department of Cardiology, Yanbian University Hospital, Yanji, Yanbian, China

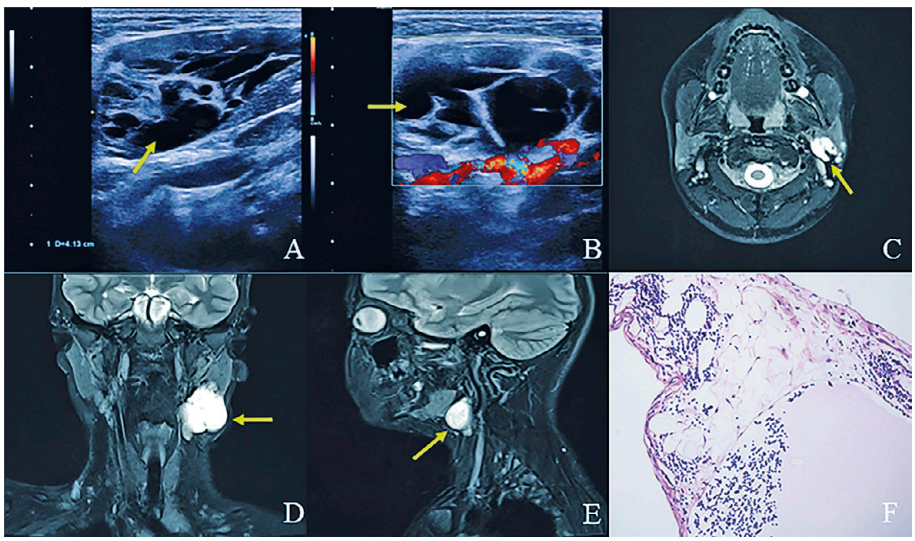


Fig 1. A) An oval anechoic mass (yellow arrow) was observed anterior and superior to the sternocleidomastoid muscle, with ill-defined borders with the parotid gland. The internal echoes of the mass were heterogeneous, and multiple hyperechoic band-like septations were seen within it; B) CDFI revealed no obvious blood flow signal within the mass (yellow arrow); C,D,E) MRI demonstrated a left-sided hyperintense mass (yellow arrow) ill-defined from the parotid gland, and T2-weighted fat-suppressed MRI showed multiple internal septa; F) Histopathological examination of the surgically excised mass revealed a lymphangioma.

To the Editor,

A 12-year-old child presented to our hospital with a slowly progressive, enlarging mass on the left side of the neck, which was first noted 10 years ago, without prior examination or treatment. Physical examination revealed a palpable mass measuring approximately 4×4×2 cm located anterior and superior to the left sternocleidomastoid muscle. The mass was firm in consistency, poorly mobile, and non-tender on palpation. No ulceration or discharge was observed on the overlying skin.

Received 08.05.2026 Accepted 26.07.2026
Med Ultrason
2026, Vol. 28, No 3, 370-371, DOI: 10.11152/mu-4639,
Corresponding author: Yihua Gao
Department of Medical Ultrasound,
Yanbian University Hospital,
#1327 Juzi St., Yanji, 133000, China
E-mail: gyh20021997@163.com
Phone: +8604332660056

Ultrasonography demonstrated an oval anechoic mass located anterosuperior to the left sternocleidomastoid muscle, measuring 4.1×4.2×2.1 cm, with an ill-defined margin with the parotid gland, heterogeneous internal echotexture, posterior acoustic enhancement, and multiple hyperechoic band-like septa within the mass (fig 1A). Color Doppler flow imaging (CDFI) detected no obvious internal blood flow signal (fig 1B). Magnetic resonance imaging (MRI) showed an abnormal cystic signal in the left upper neck, with an ill-defined boundary with the parotid gland (fig 1C,D). Fat-suppressed T2-weighted MRI showed a hyperintense mass anterosuperior to the sternocleidomastoid muscle, with multiple internal septations (fig 1D,E). The patient subsequently underwent general anesthesia and resection of a left cervical mass. Postoperative pathological examination confirmed cervical lymphatic malformation (LM) (fig 1F), and immunohistochemical analysis showed D2-40 positivity. One month later, ultrasound examination of the surgical site

revealed no abnormalities, and regular clinical follow-up was recommended.

Macrocystic LM is a rare benign developmental anomaly of the lymphatic vessels, presenting as large fluid-filled cysts. It occurs most commonly in the neck, is often detected at birth or before two years of age and progresses slowly [1]. Treatment options include pharmacotherapy, percutaneous sclerotherapy, and surgery. Patients with isolated LM have a good prognosis after treatment, and a few patients may experience recurrence [2].

In this case, the patient's lesion was poorly demarcated from the parotid gland, suggesting a possible parotid origin. Due to the lack of specific clinical manifestations, initial misdiagnosis is common. During diagnosis and treatment, attention should be paid to differentiation from branchial cleft cyst, epidermoid cyst, and pilomatricoma.

Acknowledgment: This study was supported by the Science and Technology Department of Jilin Province (No. 20200201565JC).

References

1. Mäkinen T, Boon LM, Vikkula M, Alitalo K. Lymphatic Malformations: Genetics, Mechanisms and Therapeutic Strategies. Circ Res 2021;129:136-154.
2. Huerta CT, Beres AL, Englum BR, et al. Management and Outcomes of Pediatric Lymphatic Malformations: A Systematic Review From the APSA Outcomes and Evidence-Based Practice Committee. J Pediatr Surg 2024;59:161589.

Isolated tear of the superior bundle of the subscapularis tendon: sonographic detection using the USMSIT/NMUSIT protocol

Yu-Ting Li[1], Wei-Ting Wu[1,2], Ke-Vin Chang[1,2,3], Levent Özçakar[4]

[1]Department of Physical Medicine and Rehabilitation, National Taiwan University College of Medicine, Taipei, Taiwan, [2]Department of Physical Medicine and Rehabilitation, National Taiwan University Hospital, Bei-Hu Branch, Taipei, Taiwan, [3]Medicine, Wang-Fang Hospital, Taipei Medical University, Taipei, Taiwan, [4]Department of Physical and Rehabilitation Medicine, Hacettepe University Medical School, Ankara, Turkey

To the Editor,

An 86-year-old man presented with right shoulder pain for the past month, denying preceding trauma. Physical examination showed full passive range of motion. Plain radiographs revealed no fracture or dislocation. As his symptoms had not improved with rest and analgesics, he was referred for ultrasound examination. Scanning began at the bicipital groove whereby the long head of the biceps tendon appeared swollen, but without peritendinous effusion or subluxation. With the shoulder gently externally rotated, the transducer was then moved medially along the long axis of the subscapularis tendon. From caudal to the cranial portion of the lesser tuberosity, the tendon bundles were assessed sequentially. The inferior (fig 1a) and middle (fig 1b) bundles showed a preserved fibrillar pattern, whereas the superior bundle showed a full-thickness tear with a retracted tendon stump (fig 1c). Ultrasound clearly distinguished the torn bundle from the intact anterior glenohumeral capsule. The transducer was rotated to a short-axis orientation of the subscapularis tendon (fig 1d) where only the middle and inferior bundles were visualized, and the superior bundle was not seen. The remaining rotator cuff tendons were intact. These findings were compatible with an isolated full-thickness tear of the superior bundle of the subscapularis tendon.

Isolated subscapularis tendon tears are uncommon, and most reported cases are traumatic [1]. An atraumatic, isolated tear can therefore be easily overlooked. The subscapularis tendon consists of multiple bundles and, as tears typically begin at the superomedial articular surface and progress inferolaterally, the superior portion is the

Received 29.05.2026 Accepted 26.07.2026
Med Ultrason
2026, Vol. 28, No 3, 371-372, DOI: 10.11152/mu-4640,
Corresponding author: Ke-Vin Chang, MD, PhD
Department of Physical Medicine and Rehabilitation, National Taiwan University Hospital Bei-Hu Branch, 87, Nei-Jiang Rd., Wan-Hwa District, Taipei 108, Taiwan
E-mail: kvchang011@gmail.com

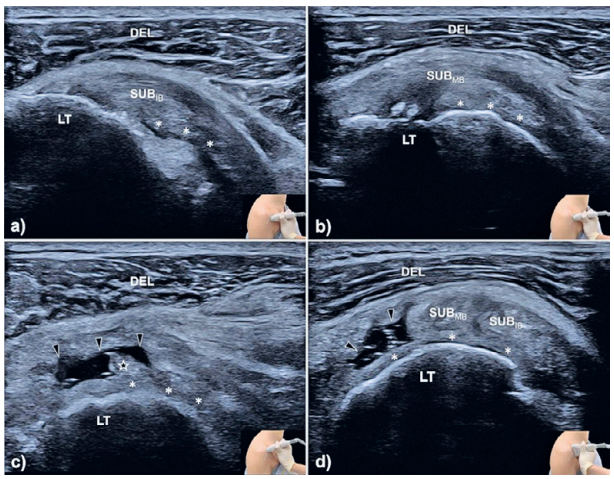


Fig 1. Systematic ultrasound evaluation of the three subscapularis tendon bundles. In the long-axis views, the inferior (a) and middle (b) bundles show a preserved fibrillar pattern, whereas the superior bundle (c) demonstrates a full-thickness tear *(black arrowheads)* with a retracted tendon stump *(star)*. In the short-axis view (d), only the middle and inferior bundles are visualized. Asterisk, anterior glenohumeral capsule; DEL, deltoid; LT, lesser tuberosity; SUBIB, inferior bundle of subscapularis tendon; SUBMB, middle bundle of subscapularis tendon.

most commonly affected site [1,2]. Because the lower and middle bundles are usually spared early, a non-systematic scan of these uninvolved bundles may lead to a false impression of normal tendon. This case highlights the importance of a structured, footprint-based scanning of the subscapularis tendon, as recommended in a recent standardized shoulder ultrasonography guideline [3].

Acknowledgment: This study was funded by the National Taiwan University Hospital, Bei-Hu Branch; the Ministry of Science and Technology, Taiwan (MOST 106-2314-B-002-180-MY3 and MOST 109-2314-B-002-114-MY3); National Science and Technology, Taiwan (NSTC 112-2314-B-002-134, NSTC 113-2314-B002-208-MY2, NSTC 113-2314-B-002-209-MY2 and NSTC 114-2923-B-002 -002 -MY3) and Taiwan Society of Ultrasound in Medicine.

References

1. Alilet M, Behr J, Nueffer JP, Barbier-Brion B, Aubry S. Multi-modal imaging of the subscapularis muscle. Insights Imaging 2016;7:779–791.
2. Chang KV, Wu WT, Tsai YY, Özçakar L. Targeting the rotator cuff and the rotator interval in shoulder pathologies. In: Chang KV, ed. Ultrasonography of usculoskeletal pain: Insights into the upper extremity. Singapore: Springer Nature Singapore; 2025:3-33.
3. Chang KV, Wu WT, Tsai YY, et al. USMSIT/NMUSIT fundamental guide on diagnostic and interventional shoulder ultrasonography. J Med Ultrasound 2026;34:1-8.

Left atrial compression caused by esophageal squamous cell carcinoma

Ling Xu[1*], Fenglin Jiang[2*]

** the authors share the first authorship*

[1]Department of Neurosurgery, [2]Department of Medical Ultrasound, the Affiliated Hospital of Yanbian University (Yanbian Hospital), Yanji, Jilin, China

To the Editor,

A 53-year-old male presented with esophageal cancer recurrence more than 8 months following surgical resection. He had a history of pT3N1M0 stage III esophageal squamous cell carcinoma, complicated by metachronous liver, lung, and pelvic metastases, and was receiving palliative chemotherapy consisting of tegafur and irinotecan in combination with sintilimab. Esophagogastroduodenoscopy revealed an esophageal space-occupying lesion, and histopathological evaluation confirmed squamous cell carcinoma. Immunohistochemical staining was positive for P40, CK5/6, and CK8/18; focally positive for CEA; negative for Synaptophysin and Chromogranin A; and showed high proliferative activity with 40% positivity for Ki-67 and aberrant overexpression of p53 (80% positivity). Echocardiography revealed a hyperechoic mass behind the left atrium, measuring 76x60 mm, with

Received 21.04.2026 Accepted 19.05.2026
Med Ultrason
2026, Vol. 28, No 3, 372-373, DOI: 10.11152/mu-4641,
Corresponding author: Fenglin Jiang
Department of Medical Ultrasound,
Yanbian University Hospital,
#1327 Juzi St., Yanji 133000, China
Phone:+86-433-2660056
E-mail: jiangfenglin@sina.com

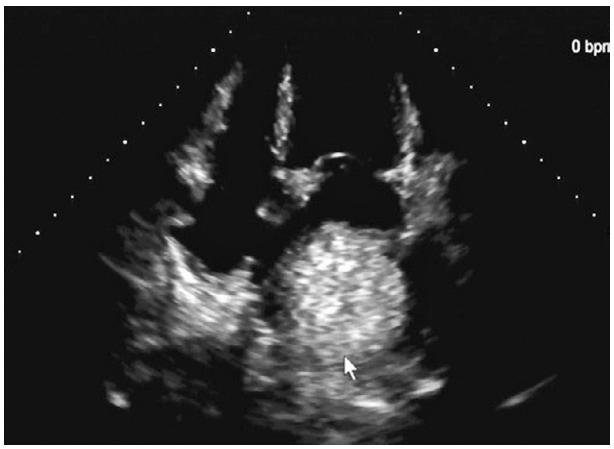


Fig 1. In the four-chamber view of the echocardiogram, a hyperechoic lesion is observed posterior to the left atrium.

ill-defined borders and an irregular shape. The internal echogenicity was heterogeneous. The mass was located between the left atrium and the thoracic aorta, compressing the left atrium, with no detectable blood flow signal (fig 1).

Esophageal cancer is one of the most prevalent malignancies worldwide. As a highly aggressive neoplasm of the upper gastrointestinal tract, it is characterized by a high mortality rate and a poor prognosis. In patients with advanced disease, progressive dysphagia and weight loss typically present as the initial clinical manifestations [1,2]. Nagatsuka et al. study [3] reported that postoperative atrial fibrillation following esophagectomy for esophageal cancer is not uncommon. Multivariate analysis identified a left atrial anteroposterior diameter ≥36 mm and an E/e' ratio ≥8.4 as independent risk factors for postoperative atrial fibrillation. Obstructive shock results from impaired cardiac output due to physical obstruction of blood flow; compression of the cardiac chambers particularly the left atrium leads to reduced end-diastolic volume and subsequent hemodynamic compromise [4]. Meanwhile, pericardial pneumatosis represents a grave complication in patients with esophageal cancer. It typically signifies advanced disease and portends a poor prognosis, with most patients succumbing to the condition within weeks [5]. In summary, patients diagnosed with esophageal cancer should undergo echocardiography as part of their clinical evaluation.

References

1. Kasim SM, Hussain S, Alsharhan MA, et al. Acute pericarditis as the presenting symptom of a case of oesophageal carcinoma. BMJ Case Rep 2024;17:e259116.
2. Chen F, Zhang J, Bai W. Establishment and Analysis of a Prognostic Model of Autophagy-Related lncRNAs in ESCA. Biomed Res Int 2022;2022:9265088.
3. Nagatsuka Y, Sugimura K, Miyata H, et al. Predictive value of preoperative echocardiographic assessment for postoperative atrial fibrillation after esophagectomy for esophageal cancer. Esophagus 2021;18:496-503.
4. Kalam S, Marquez S, Samones EJ, et al. A Case Report of Obstructive Shock from an Esophageal Bolus Leading to Left Atrial Compression. Clin Pract Cases Emerg Med 2025;9:49-52.
5. Pinto TC, Martins T, Seabra D, et al. The "airgap" and "swirling bubbles" signs in a patient with esophageal carcinoma. Echocardiography 2023;40:252-258.

A case of umbilical cord torsion diagnosed by prenatal ultrasound

Gui-lin Ye, Jia-yi Zhang, Lu Ye, Hong Luo

Department of Ultrasound, West China Second University Hospital, Key Laboratory of Birth Defects and Related Diseases of Women and Children (Sichuan University), Ministry of Education, Chengdu, Sichuan, China

Received 12.05.2026 Accepted 26.07.2026
Med Ultrason
2026, Vol. 28, No 3, 373-374, DOI: 10.11152/mu-4642,
Corresponding author: Lu Ye
Department of Diagnostic Ultrasound,
West China Second University Hospital,
Sichuan University, Chengdu,
Sichuan Province 610041, China
E-mail: cltwo@163.com

To the Editor,

A 31-year-old primigravida (G1P0) presented to our outpatient department for a routine prenatal ultrasound (US) examination at 34+4 weeks of gestation, during which marked and dense umbilical cord coiling was observed (fig 1a,b), and the estimated fetal weight fell

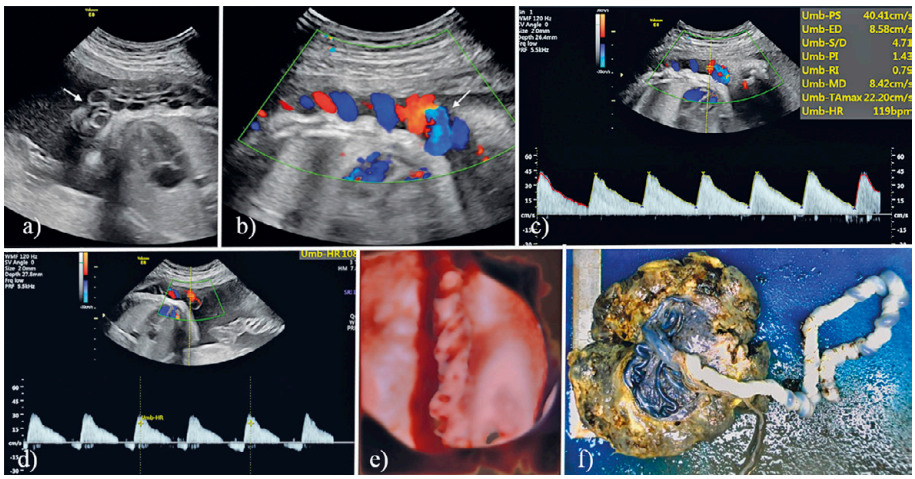


Fig 1. a,b) Gray-scale and color Doppler ultrasound demonstrated the free segment of the umbilical cord was hypercoiling and dense (arrow); c,d) spectral Doppler displayed an increase in the S/D ratio and PI of the fetal umbilical artery, intermittent end-diastolic blood flow absence and reversal, and transient slowing of the fetal heart rate; e) three-dimensional ultrasound revealed the cord straightening, tightening and hypercoiling; f) macroscopic appearance of UCT.

below the 10th percentile. Prior US examinations had demonstrated fetal growth measurements appropriate for gestational age, with no major anomalies detected. The patient had an unremarkable medical history and fetal heart rate monitoring was normal. Spectral Doppler of the fetal free loop of the umbilical cord showed an increased systolic/diastolic ratio (S/D) and pulsatility index (PI) (fig 1C): S/D=3.46-4.71, PI=1.2-1.4. Meanwhile, intermittent absence and reversal of end-diastolic flow in the umbilical arteries was also noted, accompanied by transient fetal bradycardia (108 beats per minute) (fig 1D). To rule out the possibility of temporary cord compression, the patient was placed in the left lateral decubitus position and fetal movement was stimulated. Nevertheless, the abnormalities in umbilical artery hemodynamics were not resolved after 15 minutes. Fetal middle cerebral artery and ductus venosus Doppler indices were within normal limits. Three-dimensional (3D) ultrasound imaging demonstrated the umbilical cord was significantly spiraling and tightened (fig 1e). Based on these findings, umbilical cord torsion (UCT) was diagnosed. Subsequently, a male infant weighing 2080 g was successfully delivered via emergency cesarean section, having Apgar scores of 8-10-10. The umbilical cord was about 62 cm in length and 1.7 cm in diameter, tightly twisted for 60 weeks and the UCT was verified (fig 1f).

The umbilical cord is the vital lifeline for fetal survival and development in utero, and its normal function is essential to fetal health. UCT is a rare, unexpected event in the second and third trimesters that can precipitate serious perinatal complications, including fetal distress, non-immune hydrops, intrauterine growth restriction, and even fetal demise [1]. UCT is seldom diagnosed prenatally and is usually identified through postnatal examination of the cord [2]. However, due to inherent limitations in prenatal imaging and the lack of common prenatal ultrasound findings, the diagnosis of UCT remains challenging. In previous reports, the majority of UCT cases have been seen at the fetal or placental cord insertion sites [2]. In this case, we observed significant morphological and hemodynamic abnormalities in the free segment of the umbilical cord, including tightening, hypercoiling and persistent absent/reversed end-diastolic flow. Moreover, the unexplained growth restriction of the fetus further supports the possibility of UCT, which may disrupt fetoplacental exchange and blood supply. These US findings can help to complement the prenatal sonographic features of UCT, thereby guiding early clinical diagnosis and timely intervention to prevent adverse perinatal outcomes.

References

1. Chen, N, Qiu, L, Luo, H. A case report of umbilical cord torsion: Abnormal hemodynamics of the umbilical artery assessed by ultrasound. Eur J Obstet Gyn Reprod Biol 2023;285:214-216.
2. Hashiramoto, S, Arakaki, T, Takita, H, et al. Prenatal diagnosis of the umbilical cord torsion at the placental cord insertion site: A case report and literature review. J Obstet Gynaecol Res 2024;50:1728-1731.

One case of primary thyroid myxoid liposarcoma

Lian-di Liu[1*], Ting-yi Wang[1*], Da-wei Wang[2], Lin Li[1], Jing-fang Cao[1], Shuang Zheng[1]

** the authors share the first authorship*

[1]Department of Ultrasound, Renmin Hospital, [2]Department of Ultrasound, Taihe Hospital, Hubei University of Medicine, Shiyan,China

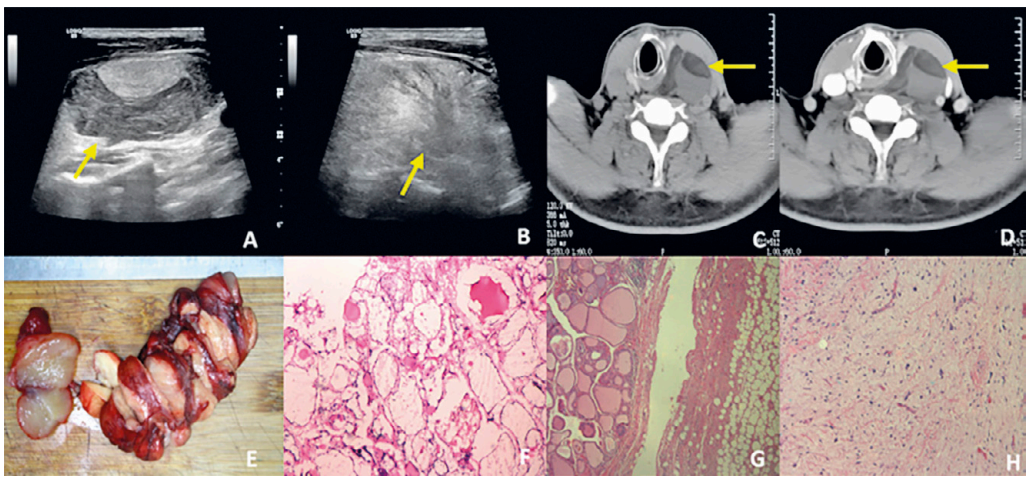


Fig 1. A, B) The left lobe of the thyroid gland is enlarged, with diffuse and uneven parenchymal echogenicity. Multiple low-echo nodules are observed within, with unclear boundaries and no obvious blood flow signals; C) CT demonstrated a mixed-density mass on the left side of the anterior cervical region and there were several round-like low density shadows in it; D) The enhancement CT showed that the left cervical mass was not obviously enhanced; E) The pathological specimen revealed a translucent mass in the left thyroid; F-H) Histopathological results indicated the presence of atypical and polymorphic cells resembling adipocytes, accompanied by mucinous degeneration in the stroma and the formation of capillary networks.

To the Editor,

Myxoid liposarcoma (MLPS) generally lacks specific symptoms and mainly presents as a slowly enlarging painless mass [1]. When the tumor is large, it compresses adjacent structures. In this case, the patient exhibited compression and displacement of surrounding tissues [2]. Due to the superficial location of the thyroid, its tumors are usually detected early.

A 42-year-old male was admitted to the hospital with a solid thyroid nodule detected half a month ago. Physical examination revealed diffuse enlargement of the left lobe of the thyroid gland with enlarged lymph nodes in both neck regions. Thyroid ultrasonography showed enlargement and heterogeneous changes in the left thyroid, with multiple nodular shadows inside, poorly defined borders, and no significant blood flow signals detected (fig 1A,B). CT demonstrated a mixed-density mass on the left side of the anterior cervical region and there were several round-like low density shadows in it (fig 1C). The enhancement showed that the left cervical mass was not obviously enhanced (fig 1D).

Based on comprehensive clinical manifestations and imaging diagnoses, the patient was suspected of thyroid cancer. With the consent of the patient and his family, a thyroidectomy with surrounding lymph node dissection was performed. Intraoperative findings showed multiple nodules in the left thyroid lobe, with unclear boundaries from the surrounding tissues. The pathological specimen revealed a translucent mass in the left thyroid (fig 1E). The pathological diagnosis was thyroid myxoid liposar-

Received 17.05.2026 Accepted 30.07.2026
Med Ultrason
2026, Vol. 28, No 3, 375-376, DOI: 10.11152/mu-4643,
Corresponding author: Shuang Zheng MD
Department of Ultrasound,
Renmin Hospital,
Hubei University of Medicine,
Shiyan 442000,
Hubei, China
mail: zhengshuang1024@163.com

coma (fig 1F-1H). No additional adjuvant therapy was administered postoperatively, and the patient has been followed without recurrence or metastasis of the tumor to date.

Acknowledgments: The work was supported by Shiyan Science and Technology Bureau of Hubei Province (No. 22Y60, No. 24Y119).

References

1. Abaricia S, Hirbe AC. Diagnosis and Treatment of Myxoid Liposarcomas: Histology Matters. Curr Treat Options Oncol 2018;19:64.
2. Baranov E, Black MA, Fletcher CDM, Charville GW, Hornick JL. Nuclear expression of DDIT3 distinguishes high-grade myxoid liposarcoma from other round cell sarcomas. Mod Pathol 2021;34:1367-1372.

Middle cluneal nerve entrapment associated with an accessory sacroiliac joint: diagnostic block and ultrasound-guided treatment

Zehra Duman Şahin, Selkin Yılmaz Muluk, Vedat Altuntaş, Tuğba Yalçın

Ministry of Health Antalya City Hospital, Department of Physical Medicine and Rehabilitation, Antalya, Turkey

To the Editor,

A 52-year-old woman presented with chronic left-sided gluteal pain refractory to analgesics, nonsteroidal anti-inflammatory drugs, and physical therapy. Computed tomography demonstrated a left-sided accessory sacroiliac joint [1] (fig 1). Physical examination revealed a positive FADIR test, marked tenderness, and a positive Tinel's sign approximately 4 cm caudal to the posterior superior iliac spine (PSIS). Therefore, a diagnostic middle cluneal nerve (MCN) block was performed at the long posterior sacroiliac ligament (LPSL) region corresponding to the S2-S3 sacral foraminal level using 2 mL of 1% lidocaine. One hour after injection, the Visual Analog Scale (VAS) score decreased by 75%, supporting MCN entrapment as the primary pain generator.

Subsequently, an ultrasound-guided MCN injection was performed using a high-frequency probe positioned over the second sacral foramen and angled obliquely to visualize the LPSL, as previously described [2]. A mixture of 1 mL betamethasone, 1 mL bupivacaine, and 2 mL saline was injected using an out-of-plane technique (Video 1, on the journal site). At 2-week follow-up, the patient reported marked improvement with a VAS score of 1/10.

MCN entrapment is caused by compression of a sensory nerve originating from the S1-S3 dorsal rami. The nerve may pass above, beneath, or through the LPSL. Proposed mechanisms include repetitive mechanical irritation, ligamentous strain, and gluteal muscle traction [3]. The accessory sacroiliac joint in the present case may have altered local loading dynamics around the LPSL,

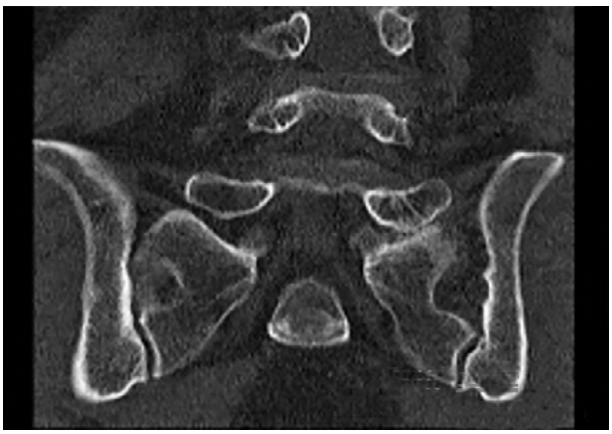


Fig 1. Coronal computed tomography image showing a left-sided accessory sacroiliac joint. Mild approximation between the left L5 transverse process and sacral ala is also noted.

Received 13.05.2026 Accepted 26.07.2026
Med Ultrason
2026, Vol. 28, No 3, 376-377, DOI: 10.11152/mu-4644,
Corresponding author: Zehra Duman Şahin
Sağlık Bakanlığı Antalya Şehir Hastanesi
Göçerler Mah. 5379 Sk.
07080, Antalya, Turkey
E-mail: zehra_dman@hotmail.com

thereby increasing susceptibility to chronic nerve irritation.

Clinically, MCN entrapment should be suspected in patients with mechanically aggravated sacroiliac region pain, particularly when tenderness or a trigger point is identified approximately 3.5 cm caudal to the PSIS. Diagnosis mainly relies on physical examination findings, especially a positive Tinel's sign, together with symptom relief following diagnostic nerve block [4].

This case highlights that accessory sacroiliac articulation may represent a previously underrecognized anatomical factor contributing to MCN entrapment. In patients with persistent gluteal pain refractory to conservative management, evaluation for cluneal nerve entrapment may help identify overlooked peripheral pain generators beyond spinal pathologies.

References

1. Teran-Garza R, Verdines-Perez AM, Tamez-Garza C, et al. Anatomical variations of the sacro-iliac joint: a computed tomography study. Surg Radiol Anat 2021;43:819-825.
2. Wu WT, Hsu YC, Mezian K, et al. Ultrasound imaging and guided intervention for the middle cluneal nerve. Med Ultrason 2023;25:119-120.
3. Karl HW, Helm S, Trescot AM. Superior and Middle Cluneal Nerve Entrapment: A Cause of Low Back and Radicular Pain. Pain Physician 2022;25:E503-E521.
4. Matsumoto J, Isu T, Kim K, et al. Middle cluneal nerve entrapment mimics sacroiliac joint pain. Acta Neurochir (Wien) 2019;161:657-661

Video 1. Ultrasound-guided middle cluneal nerve injection. LPSL: long posterior sacroiliac ligament.

Congenital vesicovaginal fistula coexisting with urethral agenesis and unilateral umbilical artery absence

Zizhuo Li, Yifei Tan, Jiao Chen

Department of Ultrasound, West China Second University Hospital, Sichuan University, Key Laboratory of Birth Defects and Related Diseases of Women and Children, Sichuan University, Ministry of Education, Chengdu, China

To the Editor

A 32-year-old pregnant woman (G1P0) presented at 32 weeks' gestation. Prenatal ultrasound revealed a 2.4x6.5x3.8 cm cystic mass posterior to the bladder, exhibiting internal low-level echoes (fig 1a). Bilateral ureteral dilatation (fig 1b), significantly enlarged bladder (fig. 1c), and absence of the left umbilical artery were noted, while the anus appeared normal. Fetal MRI suggested hydrocolpos with distal agenesis or urogenital sinus anomaly. Chromosomal microarray analysis was unremarkable.

Received 17.06.2026 Accepted 03.08.2026
Med Ultrason
2026, Vol. 28, No 3, 377-378, DOI: 10.11152/mu-4645,
Corresponding author: Jiao Chen
Department of Ultrasound,
West China Second University Hospital,
20, Renmin Road South,
610041, Chengdu,
China
E-mail: jiaochen2000@163.com

At 38 weeks, a 4600g female was delivered vaginally. Neonatal examination revealed a patent vaginal orifice and complete urethral agenesis (fig 1d). Postnatal MRI and ultrasound confirmed an elongated, fluid-distended vagina, a high-positioned uterus, bilateral ureteral dilatation, and left hydronephrosis with an enlarged, superiorly displaced bladder (fig 1e,f). Cystourethrogram and ultrasound confirmed grade IV vesicoureteral reflux (VUR) and urethral agenesis. SPECT showed left renal atrophy. Congenital vesicovaginal fistula (CVF) with urethral agenesis was diagnosed. Staged urethroplasty has been planned for post-puberty.

Congenital CVF with urethral agenesis is extremely rare. Early gestational insults likely disrupt mesonephric duct development, arresting paramesonephric duct differentiation and leading to this urogenital malformation. Typically, severe lower urinary tract obstruction often causes a severely distended bladder that terminates pregnancies via bilateral umbilical artery compression, explaining why severe CVF is predominantly diagnosed postnatally [1]. In our case, the absent left umbilical ar-

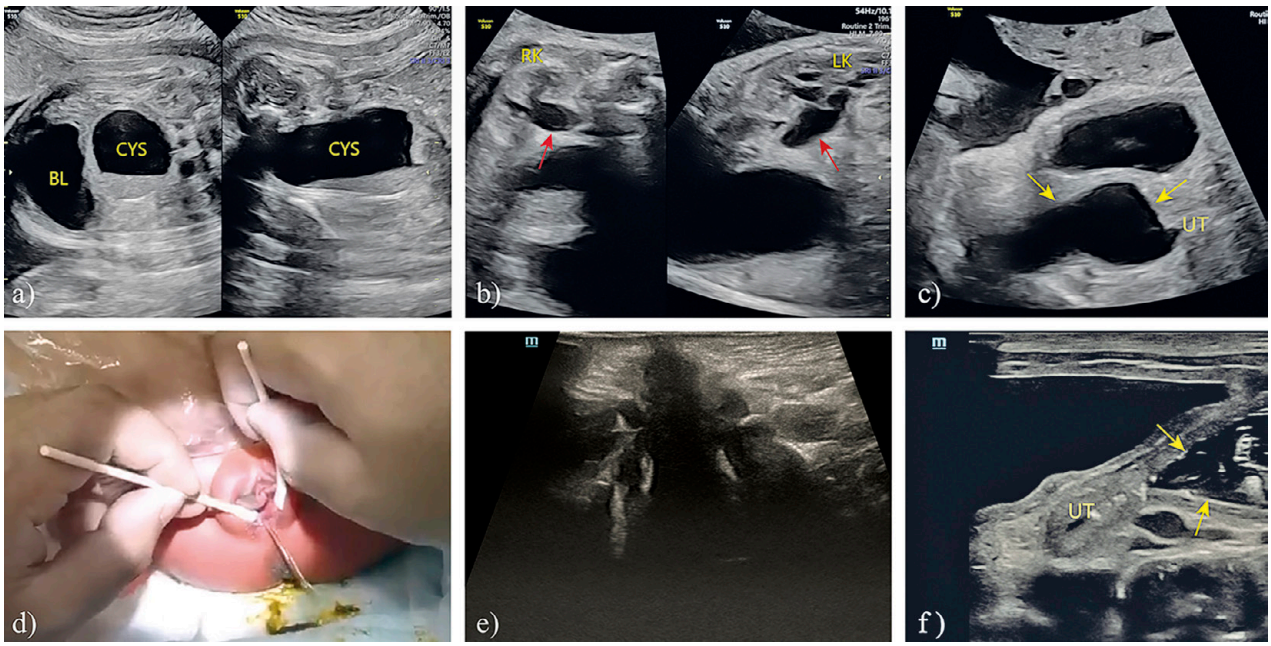


Fig 1. a) Ultrasonography showing a fetal pelvic cystic mass; b) bilateral hydronephrosis and ureteral dilatation (red arrow); c) Enlarged bladder and the fluid-filled vagina (yellow arrow); d) Urine discharge upon compression of the vaginal orifice, with absence of a urethral meatus confirmed (e); f) Fluid distension of the uterine and vaginal cavity. BL, bladder, CYS, cystic mass; RK/LK, right/left kidney; UT, Uterus; VG, vagina.

tery confirmed that high pelvic pressure had occluded one artery.

The fetus survived to term with normal amniotic fluid because the coexisting CVF and an incomplete imperforate hymen acted as a "pressure-relief valve." This created a bladder-vagina-amniotic cavity axis for urinary drainage, mitigating pelvic hypertension and preserving contralateral umbilical blood flow. Consequently, fatal pulmonary hypoplasia was avoided.

A fetal pelvic cyst posterior to the bladder with ureteral dilatation should raise suspicion for this condition. MRI fluid-fluid leveling and a normal anus help differentiate it from persistent cloaca or isolated imperforate hymen. Serial ultrasonographic follow-ups are mandatory and percutaneous vesicoamniotic shunting [2] can be considered if oligohydramnios develops. Since chronic VUR can cause insidious renal damage, prenatal multidisciplinary team evaluation and long-term surgical planning are vital for prognosis.

References

1. Rabe S, Daya M, Madaree A. Diprosopus: a review of the aetiology and case report of early surgery in a 7-week-old infant with partial facial duplication. Eur J Plas Surg 2019;42:213-222.
2. Ruano R, Safdar A, Au J, et al. Defining and predicting 'intrauterine fetal renal failure' in congenital lower urinary tract obstruction. Pediatr Nephrol 2016;31:605-612.